JOURNAL OF Applied Polymer SCIENCE

Morphological traits essential to electrospun and grafted nylon-6 nanofiber membranes for capturing submicron simulated exhaled breath aerosols

Catherine G. Reyes,[1] Margaret W. Frey[2]

[1]Physics and Materials Science Research Unit, Université du Luxembourg, Limpertsberg, L-1511, Luxembourg

[2]Department of Fiber Science and Apparel Design, Cornell University, Ithaca, New York 14853

Correspondence to: C. G. Reyes (E-mail: cgr32@cornell.edu)

ABSTRACT: As contagious bio-aerosols continue to impact our society, we examine how the morphological traits of large-scale (15 cm × 93 cm), uniformly thick, electrospun Nylon membranes can contribute to the ongoing development of diagnostic, sensor driven, face masks for capturing exhaled breath content. In our study, we compare the capture efficiencies of three types of large-scale Nylon-6 nanofiber membranes against those of commercial control textiles for capturing in-lab simulated salt breath aerosols. Furthermore, samples from the Nylon membranes were grafted with acrylic acid to determine the effects of membrane functionalization on capture efficiency. All nongrafted electrospun Nylon membranes captured 39% to 50% more salinated aerosol than the woven and nonwoven controls, despite weighing nearly 20× less. Ultimately, the nanofiber membranes were found to be far more robust during aerosol capture. Although the grafted membranes underperformed compared to the nongrafted ones, they still captured 20% to 40% more aerosol content sized between 3.5 μm and 6.0 μm (the known size range of exhaled aerosol from typical human saliva) than the woven controls. The fabrication, functionalization, and exhaled aerosol capture of these large-scale nanofiber membranes underscores the importance of assessing the lifetime, and usability, of electrospun materials before future integration with diagnostic sensing platforms can be successfully achieved. © 2017 Wiley Periodicals, Inc. J. Appl. Polym. Sci. **2017**, *133*, 44759.

KEYWORDS: electrospinning; Nylon; facemasks; textiles; breath capture

Received 2 January 2016; accepted 1 December 2016

DOI: 10.1002/app.44759

INTRODUCTION

Although many disease causing pathogens are transmittable via exhaled aerosols, studies examining the real-time airborne concentrations of infective content within these aerosols are still largely debated.[1–3] Following the reports of H5N1 infections in Southeast Asia, and the pandemic of H1N1 from 2009 to 2010, researchers questioned whether the Influenza virus was more transmittable via contact with large, settled, virus containing droplets, or via contact with suspended micron and submicron droplets originating from coughs and exhalations.[2,4,5] They ultimately found that the aerosol pathway could not be neglected as one of the more critical ways in which the virus spreads.[6–8]

H1N1, like many other viruses, can change cluster size according to atmospheric pH, temperature, and hygroscopicity—the latter influenced by the way in which virus particles may move through the nasopharyngeal passages before eventual exhalation.[9,10] While the virus can cluster to 400 nm in size, these clusters can be further augmented in saliva aerosol droplets ranging from 0.7 μm to well past 6 μm in size, if exhaled by highly symptomatic individuals.[11,12] Combined with quick changes in air flow trajectory that sneezing and coughing introduce, it makes isolating the true active concentrations, and quantifying the amount of inhalable viruses in aerosols, much more challenging.[6,10,13]

Furthermore, differentiating between viral illnesses in individuals can be problematic. While the rates of infection for many aerosol transmitted viral particles is extremely fast, the onset of disease symptoms can be delayed from 5 days to 2 weeks after the first exposure—as in the cases of measles,[14] Pertussis,[15] and influenza. The similarities in initial symptoms from these illnesses with those of the common cold, for instance, make it difficult for some adults and children to be properly diagnosed without the need for further in depth analyses.[16] By the time a proper diagnosis is determined, the infected individual will have already shown heavy symptoms at the expense of dealing with a number

Additional Supporting Information may be found in the online version of this article.

J_ID: z8e Customer A_ID: APP44759 Cadmus Art: APP44759 Ed. Ref. No.: APP-2016-10-1584.R1 Date: 31-December-16 Stage: Page: 2

of issues—i.e. waiting for laboratory diagnostic results to return, incurring costly medical bills, and delaying mass transit travel.[12,17,18]

The use of portable "point-of-care" devices, and other quick real-time methods for accurately detecting infections before the onset of heavy symptoms, and the need to perform costly tests, have the potential for greatly alleviating both the physical and socioeconomical stresses associated with aerially transmitted viral infections. Because current diagnostic devices are being developed to be portable, they also have great potential for integration with commercial wearable personal protective equipment (PPE), such as disposable face masks.[19]

To appropriately integrate portable diagnostic devices in face masks, however, an understanding of how exhaled breath content interacts with face masks and other capture devices is needed. Furthermore, experimental simulations mimicking human respiration, exhaled breath, and coughing, are necessary for modeling realistic viral aerosol transmission situations as best as possible. Although acquiring this data in laboratory settings has been difficult, studies performed by Fabian *et al.* and Diaz and Smaldone, have emulated human-like respiration and measured the capturability of exhaled aerosols using various devices.[20,21] Their studies documented the use of large animal respirators to transmit both salinated aerosols, and diluted H1N1 aerosols, to commercial protective face masks, cascade impactors, samplers, and other types of filters commonly used for capturing exhaled breath. Although Fabian *et al.* concluded that the SKC-Biosamplers® recovered nebulized viral samples with the highest preserved infectivity, in practice, such devices are bulky and complex to use.[20] Of all the capture devices tested, the Biosampler® and the cascade impactor are also not manufactured for typical consumer usage as they require professional training before operating, and are not disposable devices.

Furthermore, Diaz and Smaldone recommended that alterations to protective face mask fit and shape should be made to improve small particle deflection and capture.[21] This is a valid statement considering that although there are numerous studies on particulate and dust filtration, there are significant differences between how industrial filtration devices and disposable surgical face masks are developed. Concepts of material durability, comfortability, portability, fit, and flexibility (for withstanding fluctuations in breathing and coughing under both wet and dry conditions), become increasingly important in the design. Ultimately, such factors will influence public perception, and thus, the frequency of mask usage.[22,23]

Many studies already show that a large percentage of individuals (up to 90% even) do not know how to properly fit, or do not use, surgical masks as preventative measures against aerosol transmissions.[24,25] Thus, the effectiveness of current mask perceptions and design for the non-professional public, even without additional diagnostic components, still need reconsideration. Furthermore, while the CDC recommends the use of N95 surgical masks in occupational settings for blocking environmental particulates, its usage recommendation against bio-aerosol pathogens for the general public is still debatable.[26] Overall, continued research in surgical mask design, and materials for capturing exhaled aerosol particles and airborne droplet aggregates effectively, and cost efficiently, as well as for the development of future wearable diagnostics, is still very much needed and is of great public interest.[27–29]

Face masks comprised of polymeric nanofibers can offer viable solutions. Light weight membranes produced from fibers with nanometer sized diameters are known to be flexible, and have high surface areas, when compared to conventionally spun micron fiber nonwovens.[30–32] Furthermore, theoretical models have also shown that aerosol particle capture in nonwovens can be increased when fibers have smooth fiber lengths, smaller than micron sized diameters, and circular cross-sections.[33,34]

While nanofibers have already shown their utility as electronic sensors for sweat ion,[35] and temperature detection,[36] the detriment to these devices is that they require the use of extra electronics, and professional expertise to accurately interpret the results. Earlier in 2016, Guder *et al.* introduced a cellulose paper-based diagnostic for face mask integration which, although highly functioning, also eventually suffered from high power usage, and potential paper degradation.[37] Alternatively, nanofiber membranes produced from textile grade polymers—such as Nylons are shown to be quite robust, and efficient (particularly when nanofiber diameters are closer to 120 nm[38]). They have the potential for addressing the issues of fit, durability, and aerosol capture while providing a platform for enhancing diagnostic capabilities at the same time. Furthermore, the use of colorimetric, and lateral flow assays, readable via color changes are far more attractive for nanofiber membrane use, as they can function without battery supplements.[39,40] By far, the most economically flexible way to produce nanofiber membranes is through the electrospinning process.[41,42] Nearly all aspects of the production, from solution to fabrication related parameters, are controllable by the experimentalist—thus, enabling the fast production of tailored nanofiber membranes with selected morphologies, and functional attributes.[43–47]

Therefore, taking into consideration the need for improvements in current face mask design and materials, the existing time-related difficulties in diagnosing airborne transmitted illnesses, and the known ability to fabricate textile grade polymers into nonwovens via the electrospinning process, we report on the simulated exhaled salt aerosol capture efficiencies of membranes extracted from three large scale (15 cm × 93 cm), and uniformly thick, electrospun Nylon sheets containing fiber diameters ranging from 100 to 150 nm, against that of commercial woven and nonwoven textiles. The size percentages of aerosol salt captured are also reported. According to known literature regarding experimental simulations of exhaled breath generation, the exhaled aerosol capture studies presented here were performed using a large animal respirator which created saline aerosols with droplets ranging from 0.25 μm to over 6 μm in size.

We also examine the effects that acrylic acid grafting had on the capture efficiencies of the electrospun membranes, and discuss whether the capture efficiencies of the electrospun could be further tuned for targeting specific size ranges of airborne particulates by using this quick, although somewhat harsh, surface

ID: kannanb Time: 13:26 I Path: //chenas03/Cenpro/ApplicationFiles/Journals/Wiley/APP#/Vol00000/161191/Comp/APPFile/JW-APP#161191

J_ID: z8e Customer A_ID: APP44759 Cadmus Art: APP44759 Ed. Ref. No.: APP-2016-10-1584.R1 Date: 31-December-16 Stage: Page: 3

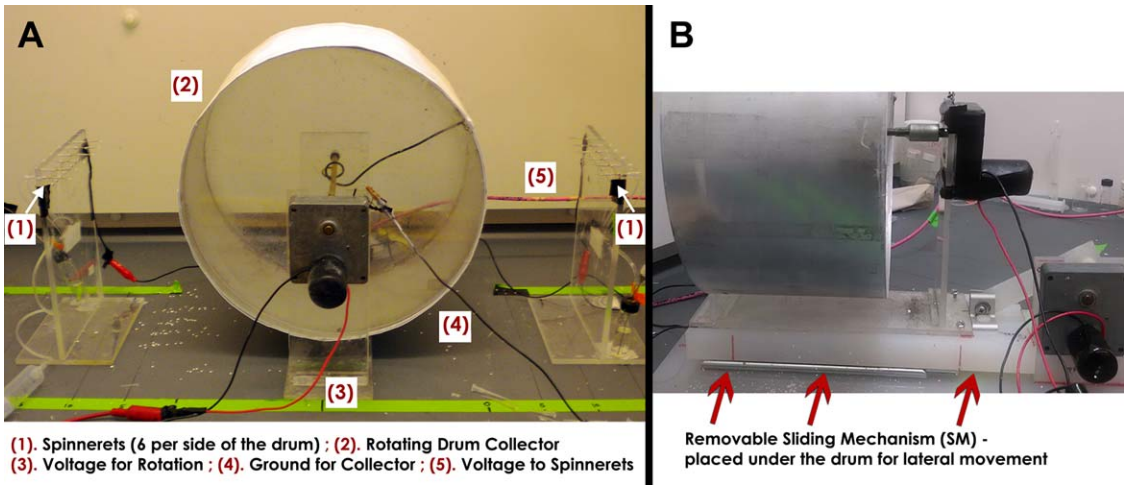

Figure 1. The full electrospinning setup, without the lateral sliding mechanism, is shown in (A) with the rotating drum collector in the center and 12 spinnerets, six on each side, facing it. The snapshot of the drum in (A) was taken while the spinning process was occurring, and shows the development of a representative, white, Nylon-6 nanofiber membrane. A side profile of the drum collector with the lateral sliding mechanism is shown in (B). The sliding base can be attached and removed as desired. [Color figure can be viewed at wileyonlinelibrary.com]

treatment step. Finally, we discuss the resulting impacts on membrane durability, and performance.

EXPERIMENTAL

Nylon-6 Nanofiber Membrane Fabrication

Solutions for Spinning. Nylon-6 pellets (MW: 12,112 g mol^{-1}) were obtained from Sigma-Aldrich (Product #181110) and dissolved in formic acid (88%, Macron Fine Chemicals) to create three separate polymer solutions containing 20 wt % Nylon each. The total volume of each vial was 7 mL—this was the minimum amount of 20 wt % Nylon-6 solution volume required to electrospin one uniformly thick, large scale (15 cm × 93 cm) Nylon-6 nanofiber membrane using the multi-spinneret and rotating drum system further described in the Gamma Irradiation Grafting Process section. All three solutions were left shaking overnight in a Wrist Action Shaker (Model 75, Burrell Scientific) until the Nylon-6 was thoroughly and homogenously dissolved. The solutions were clear in appearance, and were not altered further before spinning.

Components of the Large-Scale Electrospinning Setup. The prepared Nylon-6 solutions were electrospun onto a large aluminum foil covered drum (diameter 28 cm; side length 15 cm; with Dayton Motor Model# 2L011-50RPM) by using twelve (22-gauge) blunt end stainless steel needles as spinnerets (obtained from Whilson's Hardware Store, www.whilson.com; Part #NE-223PL-25). The needles and drum are labeled (1) and (2), respectively, in Figure 1(A). A set of six needles were supported on each side of the rotatable drum using two acrylic stands. The use of 12 needles was necessary to ensure uniform macroscale fiber deposition onto the full width of the drum.

The electrospinning process was carried out three times to create three large nonwoven Nylon membranes according to the parameters shown in Table I. Thus, the membranes are referred to in the text using their abbreviated names. We chose to vary the parameters related to collector motion, and collector distance, because these are variables known to make significant differences in nanofiber nonwoven morphology when the solution properties are kept constant. We electrospun two membranes, each with needle distances of 10 cm from the rotating collector, and one membrane at 12.5 cm distance.

First, for creating the 10CM NSM membrane, the two needle stands facing the drum were offset from each other by 3 cm. This was done so that a completely uniformly covered fiber membrane could be produced over the entire width of the drum without "band stripes" of uncovered area developing. "NSM" describes the membrane produced without the additional laterally sliding component. Figure S.1(B) of the Supporting Information shows a photograph of the entire length of this membrane that is produced.

Second, for determining whether adding collector motion, without offsetting the needle stands, would change the quality of the large-scale membranes produced, we spun 10CM SM and 12.5CM SM onto the drum with added lateral motion. This slightly different drum configuration using an axial sliding base, abbreviated as "SM" in Table I, and shown in Figure 1(B), was operated using the same 12 spinneret needle configuration. The removable laterally sliding base was created from a 2 cm thick acrylic base mounted over sliding rails attached to a flat bottom. The base was pushed and pulled laterally by an acrylic "arm" piece attached to a DC Dayton gear motor (Model# 2L011–50RPM).

The Electrospinning Process. To electrospin one large Nylon sheet, one Nylon solution was equally divided into two smaller vials each containing a septum top—carefully making sure that at least ½ cm of headspace in each vial was present. These septum covered vials were placed on each needle stand, under each six-needle set facing the rotating cylinder. Two syringe needles (18-gauge) were inserted into each septum covered vial—one terminated in the headspace above the Nylon solution, and the other was fully immersed in the solution. The top ends of the former needles terminating in the vial headspace, were

ID: kannanb Time: 13:27 I Path: //chenas03/Cenpro/ApplicationFiles/Journals/Wiley/APP#/Vol00000/161191/Comp/APPFile/JW-APP#161191

J_ID: z8e Customer A_ID: APP44759 Cadmus Art: APP44759 Ed. Ref. No.: APP-2016-10-1584.R1 Date: 31-December-16 Stage: Page: 4

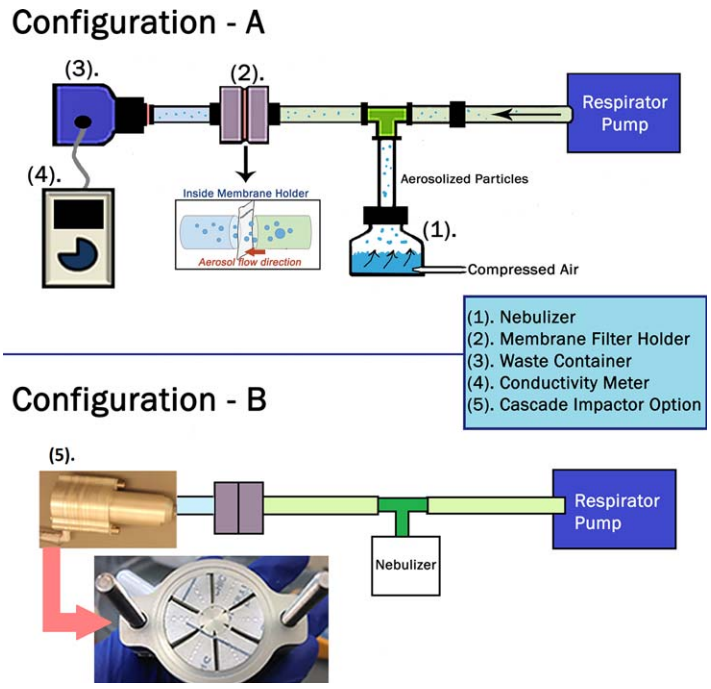

Figure 2. Two diagrams of the configurations possible for assembling, and acquiring two different types of data from the Simulated Breathing Apparatus are shown. Configuration (A) has the waste container-conductivity meter collection device terminating the apparatus. The filter membrane holder shown in (2) shows a close-up of how the capture membrane between the ends of the aerosol transport hoses appears. Configuration (B) shows the breathing apparatus terminating with the cascade impactor size and weight collection device. An example of a stage within the impactor used to collect the aerosol is shown in the inset photo. [Color figure can be viewed at wileyonlinelibrary.com]

connected via tubing to two empty syringes (60 mL capacity) held in a dual syringe pump (Harvard PHD, Ultra Harvard Apparatus Cat. #170–3005). The top ends of the latter needles immersed in the solution, were connected via tubing to a stainless steel fluid manifold with six channels (Small Parts Inc., Model #STCM-13-20/6). This manifold connected to each of the six electrospinning needles places on each side of the cylinder. Figure S.1(A) in the Supporting Information shows a detailed image showing the setup described here.

The syringe pump was set between 0.2 and 0.3 mL hr^{-1} to pump air into each septa covered vial. As the septum covered vials became pressurized, the polymer solution flowed into the immersed needle through the manifold, and into each of the needles simultaneously via capillary flow. Copper wire wrapped around each needle leading to the high voltage clip of the voltage box facilitated the spinning process. The ground was connected to the rotating cylinder collector itself. The Heathkit Model #Sp-2717, and Gamma High Voltage Research Model #ES30P-5W voltage units were used for rotating the drum, and driving the electrospinning process, respectively. Though these units are not shown in Figure 1(A), the wire connections are as follows: red and black wires (3) from the drum were connected to the Heathkit unit, the red and black wires in the back linked to the needles (5), were connected to the gamma unit. All electrospinning was performed at 27 kV and 5 kV, for the gamma unit and Heathkit unit, respectively.

Table I. The Three Types of Large-Scale Nanofiber Membranes Electrospun Based on differences in Processing Parameters: Needle-Tip-to-Collector Spinning Distance in Centimeters, and Collector Sliding Motion (SM)

Spinning distance (cm)	SM?	Membrane name
10	No	10CM NSM
10	Yes	10CM SM
12.5	Yes	12.5CM SM

The names given to each membrane reflect the parameters chosen for its production.

All three nanofiber membranes were spun for approximately 4 hours each, at a temperature of 25 °C, and a relative humidity of 30% to 35%, until the drum was uniformly, and entirely covered with the nonwoven Nylon mat. To further check each membrane's thickness, samples were removed from each sheet for microscopic analysis using field emission scanning electron microscopy (FESEM), the results of this are shown in Figure S.3(C) of the Supporting Information.

Simulated Breathing Apparatus and Aerosol Capture Process

Two configurations of the simulated breathing apparatus were used to capture, disperse, and monitor the salt aerosols in this study. Line drawings of both are shown in Figure 2(A,B)— F2
where the former configuration was used to determine concentration of salt aerosol captured, and the latter configuration was used to quantify the size percentage of aggregated particles captured. Both configurations are similarly assembled, except for the differences in the devices terminating at the end. In the first configuration [Figure 2(A)], a respirator pump (Harvard

ID: kannanb Time: 13:27 I Path: //chenas03/Cenpro/ApplicationFiles/Journals/Wiley/APP#/Vol00000/161191/Comp/APPFile/JW-APP#161191

J_ID: z8e Customer A_ID: APP44759 Cadmus Art: APP44759 Ed. Ref. No.: APP-2016-10-1584.R1 Date: 31-December-16 Stage: Page: 5

Apparatus, Model #B-55172) was connected to the main hose line, and to a nebulizer bulb (1). The nebulizer bulb contained a sodium chloride solution, and was connected to a compressor (Medline Aeromist Plus Nebulizer Compressor, Model #MED-HCS60004) providing air to aerosolize the solution. The aerosol that flowed through the hose line was be captured by a suspended membrane housed in the filter holder (2). Uncaptured aerosol traveled into a waste container (3) containing deionized water (acquired from: EMD Millipore Milli-Q, 18.2 mΩ) at the end of the setup. A conductivity meter (IQ Scientific Instruments, Model #IQ170) (4) was placed in the waste container to measure the change in water conductivity as uncaptured aerosols accumulated in the waste container. From these conductivity values, the amount of salt aerosol capturable on each membrane tested was back-calculated.

The second configuration, Figure 2(B), was assembled in exactly the same manner as shown in Figure 2(A), except for the replacement of the conductivity meter (4) with the cascade impactor (5). The cascade impactor (Marple Series 290–8 with inline adaptor: 290-I-A) was used for quantifying the size range of salt aerosol droplets dispersed throughout the system. The weight of each stage in the impactor was taken before and after salt aerosol dispersion. First, salt aerosol was dispersed into the whole breathing apparatus with the attached impactor several times, without the filter membrane present. This was to determine the base maximum values of weights and sizes of aggregated salt particles capturable inside the impactor. Then, the salt aerosol was dispersed throughout the system with the filter membranes present. The differences between the weights found for each size range measured by the impactor before, and after a filter membrane was introduced, described the amount of aggregated salt particles captured onto the membranes. Each stage of the cascade impactor had 34 mm diameter substrates laser cut from parafilm (Pechiney Plastics, Type M film) using a Kern Laser System with a single 150 watt laser (Model HSE 52 ×100). The inset image in Figure 2(B) shows an example of one cut substrate laid over one cascade impactor stage. More information regarding this analysis can be found in the Supporting Information, Figure S.11(A,B).

The final three membranes tested for simulated breath capture, and housed in the filter holder (2) in Figure 2, were: the three types of electrospun Nylon-6 samples, the acrylic acid grafted electrospun samples, commercial nonwoven cellulose filter papers (Whatman®, Type 1), and commercial woven polyester chiffon fabrics (purchased from JO-ANN Stores, LLC).

Gamma Irradiation Grafting Process

Gamma irradiation was used to initiate the grafting process on the membranes. Because the reactions performed required membrane exposure to both acrylic acid monomer (pH ~2), and gamma irradiation, the strongest electrospun membranes (10CM NSM and 10CM SM) evaluated from the tensile tests shown in Figure 6 were used. Strips from the two original 15 cm × 93 cm sheets were cut, and added to 10% solutions of acrylic acid monomer (obtained from Sigma-Aldrich, anhydrous) in deionized water (18.2 mΩ, obtained from an EMD Millipore Milli-Q device) volumetrically. One strip was added per vial containing acrylic acid. The vials containing both the Nylon strips and acrylic acid were irradiated using a Nordion International Gamma Cell 1000 irradiator (source: Cs-137, dosage: 523 rad min^{-1}) for 1 min, unless otherwise indicated. The Nylon-6 strips were removed from solution, washed with deionized water, spread flat to avoid folding, and left to dry in air overnight.

Membrane Characterization Techniques

Fiber diameters were examined using a Zeiss Leo 1550VP FESEM with a 20 mm aperture, working distance: 10 mm to 12 mm, and accelerating voltage: 2 kV. All samples were carbon coated using a Denton Vacuum, BTT-IV Evaporator prior to imaging. Interfiber, mesh-hole size measurements were performed independently using both SEM image analysis via Image J software from the National Institute of Health (image.j.nih.gov/ij/), and experimental testing via capillary flow porometer (Porous Materials Inc., Model #1100-AEHXL). As an aside, we refrain from using the terms "porous" and "porosity" to describe the interfiber openings within the nonwoven, and woven, materials presented in our study. Instead, we use the terms "mesh-hole opening" to disambiguate our reference from the type of intrastructural pores typically found in molecular sieve materials and individually porous fibers, such as shown by Lu and Xia.[46]

BET surface area analysis was conducted using a Gemini VII 2390 Surface Area Analyzer equipped with Ultra High 5.0 Grade Purity Nitrogen (Airgas Part #NI UHP300). The relative pressure range (P/P_0) for calculating the BET surface areas of the samples was between 0.005 and 0.18. A Nicolet 560 Magna-FTIR spectrometer with an ATR accessory was used to observe bond structure before and after the grafting reactions. The tensile (Young's modulus) of each electrospun membrane was found using the maximum stress and strain observed at each material's yield point, according to guidelines presented in ASTM D882–12 using an Instron 5566 (with 1000 N load cell, and strain rate: 1 mm min^{-1}).

RESULTS

Changes in Salt Waste Conductivity Correlate to Membrane Capture Efficiency

Using configuration A of the simulated breathing apparatus in Figure 2, the conductivity changes observed in the waste container before, and after the capture membranes were inserted in the filter holders, were compared. Figure 3(A) shows the average change in conductivity observed in the waste container, for each membrane put in the filter holder as a function of the total aerosol dispersal time. Before each 45-min aerosol dispersal session, for each membrane tested, the conductivity meter in the waste container was zeroed to make sure that any stable observed changes in the deionized wastewater container were due to only aerosols entering the container. The relative amount of exhaled aerosol unable to be captured by the membrane, and passing into the waste container, correlated to the how effective each membrane was for intercepting the nebulized aerosols. The higher changes in conductivity observed in the waste container indicated less content captured overall, and vice versa. These changes in conductivity would relate back to a mass per volume, and percentage efficiency, that the membranes could capture, F3

ID: kannanb Time: 13:27 I Path: //chenas03/Cenpro/ApplicationFiles/Journals/Wiley/APP#/Vol00000/161191/Comp/APPFile/JW-APP#161191

J_ID: z8e Customer A_ID: APP44759 Cadmus Art: APP44759 Ed. Ref. No.: APP-2016-10-1584.R1 Date: 31-December-16 Stage: Page: 6

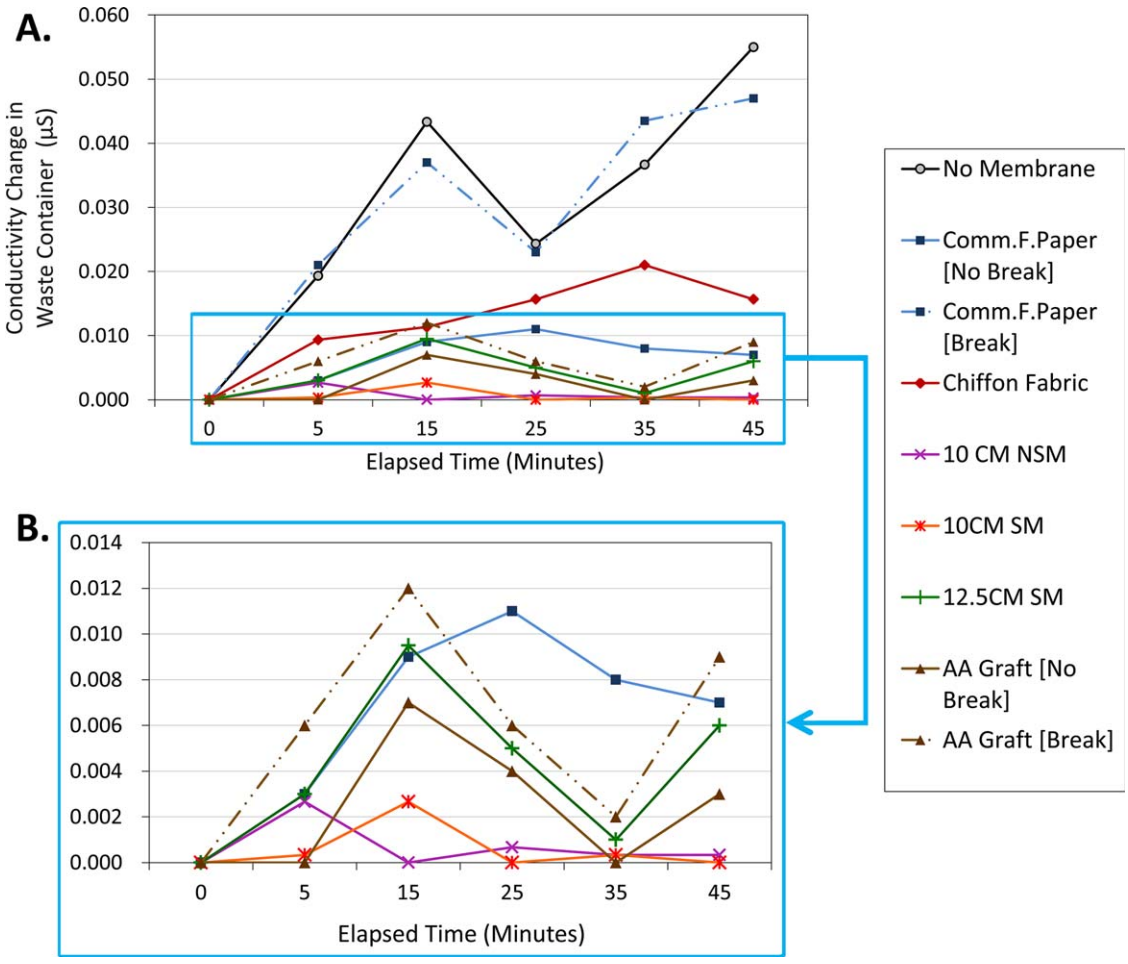

Figure 3. The waste conductivity changes observed for various membranes capturing exhaled salt aerosol. The waste conductivity changes for all membranes tested are shown in (A). The "No Membrane" curve refers to the conductivity changes associated with aerosol dispersed through the system without a capture membrane present, and it also represents the background error of the device. The close-up of the specific conductivity changes observed for the electrospun Nylon materials are shown in (B) compared to those of the unbroken commercial filter paper. [Color figure can be viewed at wileyonlinelibrary.com]

F4 shown in Figure 4. Because the least amount of conductivity changes were observed for the electrospun materials, outlined in the blue rectangle of Figure 3(A), to visualize the full scale of these changes they were plotted separately in Figure 3(B).

Perhaps the most striking results initially observed were that the commercial Whatman filter paper (labeled: Comm.F.Paper), and the acrylic acid grafted electrospun membranes (labeled: AA Graft), in Figure 3(A), physically degraded during the salt aerosol loading process, and ruptured very early before the 45-min dispersal sessions finished. All membranes had been tested for aerosol loading at least three times each. For the Whatman filter paper and the grafted membrane, we observed breakage occur at least 50% of the time during aerosol capture. For this reason, we plotted the average trends in conductivity change for those grafted and commercial filter papers which broke during capture (labeled "break"), against those which did not (labeled "no break").

Aside from physically seeing the broken membranes in the filter holders of the apparatus after stopping the aerosol dispersal, another indication that the samples broke during aerosol capture was the constant doubling of conductivity values observed for the "Break" samples compared to the "No Break" ones, at each 5-min mark for the same sample types tested continuously. This consistent trend, seen in Figure 3(A), shows that the breakage observed in the grafted and commercial filter membrane types was not merely due to experimental error, such as from the membranes shifting out of place during capture, or that the samples broke during filter holder disassembly prior to each testing session.

Additionally, while we did also observe some small rips develop in the electrospun 12.5CM SM membrane during capture, these rips and tears were not at the same level of breakage which occurred for the commercial filter and grafted samples. This is also reflected in the percentage capture results found for each membrane shown in Figure 4.

Finally, for determining the amount of salt aerosol captured on each membrane, eqs. (1) to (3), extrapolated from salt-conductivity-to-salt-concentration plots compiled for sodium chloride in deionized water, were used.

ID: kannanb Time: 13:27 I Path: //chenas03/Cenpro/ApplicationFiles/Journals/Wiley/APP#/Vol00000/161191/Comp/APPFile/JW-APP#161191

J_ID: z8e Customer A_ID: APP44759 Cadmus Art: APP44759 Ed. Ref. No.: APP-2016-10-1584.R1 Date: 31-December-16 Stage: Page: 7

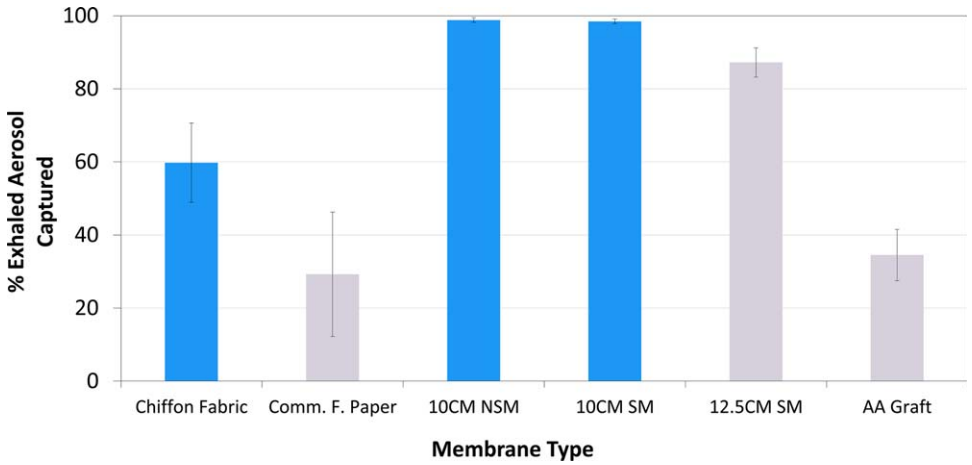

Figure 4. The percentage of aerosol captured on all of membranes is shown. All of the membranes which did not tear, or completely rupture, during aerosol capture are shown in blue bars. The gray bars indicate that these membranes were susceptible to breaking during aerosol capture. The error bars indicate the 95% confidence interval range for the amount of aerosol that can be captured by each membrane type. For the actual concentration values capturable by each membrane compared to the maximum concentration of salt aerosol that the breathing apparatus can "exhale" for a 45-min session, refer to Figure S.10 of the Supporting Information. [Color figure can be viewed at wileyonlinelibrary.com]

$$X_{WC}\ (\text{or}\ X_{NC}) = \left(\frac{Y_{Conduct} - 0.0019}{0.0036}\right) \quad (1)$$

$$M_{Captured} = X_{NC} - X_{WC} - E_{SBA} \quad (2)$$

$$\%M_{Captured} = \left(M_{Captured}/X_{SBA}\right) * 100 \quad (3)$$

Briefly, eq. (1) describes the conversion process between the different conductivities ($Y_{Conduct}$) of the aerosol collected in the waster chamber (X_{WC}), and the conductivities of the starting aerosol in the nebulizing chamber (X_{NC}), to concentration quantities. Equation (2) describes the amount of salt concentration captured per membrane after differences in the chambers, and the error of the device was accounted for (E_{SBA}). Equation (3) describes the final percent of aerosol captured on the membrane as a function of eq. (2), and the total concentration of aerosol throughput possible in the apparatus for the 45 min it is used per trial (X_{SBA}). Further details on these calculations, and the constant (X_{SBA}) are discussed in the text accompanying Figure S.9(A,B) of the Supporting Information.

Figure 4 shows the percentage of captured aerosol per membrane, based on the total amount of aerosol throughput possible in the empty simulated breathing apparatus chamber. The error bars shown consider if the membranes ruptured, or ripped during use, and reflect how well each membrane type could perform for repeated exhaled aerosol capture. For instance, although one could expect the commercial filter membranes to outperform the electrospun Nylon, as they are thicker, the commercial membranes could only capture about a third as much aerosol, capturing 39% to 50% fewer particles (if their tendencies to break during use are considered). Additionally, the commercial filter papers underperformed compared to the woven chiffon fabric (Figure 4). Both of these results can be explained by the fact the filter papers were prone to rupture from their lack of flexibility when moist, low surface area, and non-uniform fiber sizes present.

Furthermore, though the 12.5CM membranes also had tendencies to rip, their aerosol capture was still significantly higher than for the commercial filters. Compared to the two 10CM samples, however, which performed the best, and did not break during the process, capture was about 15% less for the 12.5CM type.

The grafted membranes also underperformed, capturing less than 50% of aerosol compared to the 10CM samples. Though the grafting process produced acrylic acid functionalized Nylon-6 membranes, the exposure to acrylic monomer and the effects of gamma irradiation during the grafting process, ultimately lowered their robustness, strength, and made the membranes brittle. It is important to note, that while these grafted membranes did underperform overall in aerosol capture trials, and would not be suitable for face mask integration, they did show over 80% capturability for particles sized at 6.0 μm, and 1.55 μm, as observed from the cascade impactor trials (Figure 5). F5

Captured Aerosol Particle Size Ranges on Membranes

When the sizes of captured particles from the exhaled aerosols are considered, the grafted membranes faired far better than the commercial Whatman filter paper. In the forthcoming sections, we further discuss the trade-offs seen between material durability, and enhancing smaller particle capture, when functionalizing the electrospun Nylon membranes. As shown in Figure 5, the nongrafted electrospun membranes (10CM NSM, 10CM SM, and 12CM SM) were far more superior for capturing 60% to 95% of particles smaller than 0.52 μm in size. In fact, the specific surface areas, tensile strengths, and mesh-hole sizes of the membranes were significant contributing factors for their better capture performances.

Overall, these results are significant because aerosol content sized between 0.7 μm and 6 μm is known to be the primary cause of respiratory illnesses in children and adults.[12,48] Regular nasal breathing itself causes up to 90% of particles sized between 2 μm and 20 μm to become lodged within the upper

ID: kannanb Time: 13:27 I Path: //chenas03/Cenpro/ApplicationFiles/Journals/Wiley/APP#/Vol00000/161191/Comp/APPFile/JW-APP#161191

J_ID: z8e Customer A_ID: APP44759 Cadmus Art: APP44759 Ed. Ref. No.: APP-2016-10-1584.R1 Date: 31-December-16 Stage: Page: 8

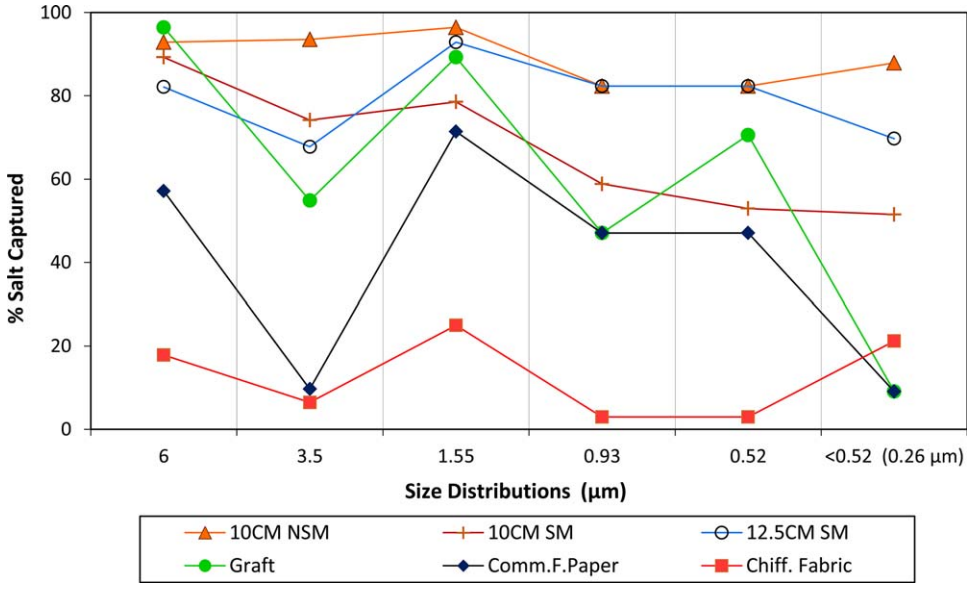

Figure 5. The weight percent of captured salt from aerosol droplets exhaled by the simulated breathing apparatus on different membranes is shown. [Color figure can be viewed at wileyonlinelibrary.com]

nasal and lower bronchi level respiratory passages.[3,49] Because up to 80% of these particulates are cleared through exhalation within 24 h, these particles can be easily converted into exhaled aerosols and also easily transmitted elsewhere. For reference, most exhaled saliva droplets can range from 0.74 µm to 15.9 µm in size.[11,49] From the cascade impactor data presented here, the particulate matter that our nanofiber media can capture is well within these aforementioned size ranges of exhalable saliva, and airborne transmittable content.

Most widely available protective face masks are useful for typically capturing exhaled aerosol droplets greater than 5 µm in size, have limited effectiveness for capturing finer particles from 0.89 µm to 3.0 µm,[24] and are known to have fitting, and comfort issues.[24,50] Furthermore, the research for integrating nanofiber based membranes with current surgical mask media for dual use purposes like aerosol particle capture coupled with diagnostic assay capabilities is still in its infancy. From our overall aerosol capture efficiency results, and the specific particle sizes capturable, large-scale fabricated electrospun Nylon membranes show potential for future integration with face masks for developing new point-of-care diagnostic tools.[50]

DISCUSSION

Why Did the Commercial Nonwoven Controls Perform Poorly?

For now, we set aside the discussions surrounding the performance of the non-functionalized electrospun membranes, as well as the grafted membrane performance, to the sections entitled: Nongrafted Electrospun Membranes Outperform the Commercial Controls, and Grafted Membrane Properties Reduce Sustained Aerosol Capture, respectively. Here, we discuss the stability failures of the commercial Whatman filter control.

Despite the fact that the commercial Whatman filter paper is able to perform well, contributing only up to 0.011 µS of salt aerosol to waste at its best [blue solid line, Figure 3(A)], if it does rupture during aerosol capture, the amount of aerosol passing through the membrane itself contributes to highly fluctuating conductivity increases observed in the waste container. The waste conductivity changes observed appear most similar, in fact, to the conductivity changes seen if there were no capture membrane present in the system at all [black line, "no membrane," Figure 3(A)]. It suggests that while the Whatman filter can be used for capturing some amount of aerosol, ultimately, this conventional paper material is neither very durable for withstanding continuous wet aerosol loading, nor the stresses associated with typical exhalation-inhalation patterns.

This was somewhat surprising because although the Whatman commercial filter is made of cellulose fibrils, the structure itself is much thicker, and sturdier, than that of the other electrospun materials tested (i.e. 10CM NSM, 10CM SM, and 12.5CM SM). For the same 45 mm diameter sized circle, the weight of one electrospun membrane (10CM NSM, in this comparison) only weighs about 6.7% of the weight that one commercial Whatman paper weighs. While the electrospun membranes are still able to be handled (i.e. picked up, folded, flattened), it would seem on the basis of weight alone that the nanomembranes would be less robust to aerosol capture than the Whatman filter. Furthermore, Whatman 1 filter paper has been extensively used for creating advanced quantitative protein assays requiring prolonged and excessive exposure to alcohols, dyes, and other organic solvents.[51] Therefore, the degradability that this filter membrane showed against a sodium chloride solution at room temperature was not expected to be as high as it was given its recent uses in other studies.

Ultimately, we believe that the properties contributing most to the failure of the commercial Whatman paper were: its very low surface area, nonuniform mesh-hole opening, and inflexibility to withstand the aerosol fluctuations the simulated breathing

ID: kannanb Time: 13:28 I Path: //chenas03/Cenpro/ApplicationFiles/Journals/Wiley/APP#/Vol00000/161191/Comp/APPFile/JW-APP#161191

J_ID: z8e Customer A_ID: APP44759 Cadmus Art: APP44759 Ed. Ref. No.: APP-2016-10-1584.R1 Date: 31-December-16 Stage: Page: 9

Table II. The BET Calculated Specific Surface Area (SSA) Determined for Various Membranes used in Aerosol Capture Studies, Compared Against that of an inner Material from a Known Commercial Face Mask Sample

Membrane type	SSA (m^2 g^{-1})	Errors (m^2 g^{-1})
10CM NSM	58.11	1.48
10CM SM (fully dry)	44.27	0.71
10CM SM (semi-dry)	20.92	0.21
12.5CM SM	57.11	1.87
Graft	9.16	0.10
Comm.F.Paper (Whatman)	2.20	0.03
Face mask inner	0.25	0.14

The respective isotherms are included in Figure S.8 of the Supporting Information.

process presented. Even after the aerosol capture trials, the textures of all broken and nonbroken filter membranes showed significant signs of wear, and fiber pilling.

The BET specific surface areas for seven membranes are shown in Table II. In particular, the commercial Whatman filter paper only had about 2 m^2 g^{-1} of available surface, while the nongrafted electrospun membranes showed areas between 40 and 60 m^2 g^{-1}. The value of 20 m^2 g^{-1} attained for a sample of the electrospun membrane 10CM SM was due to insufficient drying after production ("semi-dry"). Notwithstanding, the area is still much larger than that of both the areas found from the commercial samples presented here, even for higher masses of sample used. As a side note, the surface area for the woven chiffon fabric was not compared because, as we found after our aerosol capture studies, this material contained wide openings between fibers to begin with. As confirmed by both capillary flow porometry, and SEM image analysis, it had a mean mesh hole diameter size of about 111 μm [Figure 8(B), and Figure S.7 in the Supporting Information].

Although this fabric performed better than the nonwoven commercial Whatman filter paper, we determined this was more due to the flexibility of the fabric in withstanding the aerosol dispersal process, than the individual fiber properties in the fabric. Though the woven structure helped in adding robustness, in Figure 3(A) we observed that the conductivity changes for the chiffon fabric (red line) eventually became similar to that of the unbroken commercial Whatman nonwovens, and it also underperformed at the 35-min mark. Thus, we expected the chiffon fabric to have a much lower surface area than even the commercial Whatman paper, which was found to have a surface area of only 2.19 m^2 g^{-1} for about 57 mg of sample measured.

Instead, we compared the surface area of the inner nonwoven poly(propylene) material extracted from a 3-ply, procedural face mask sold by Kimberly-Clark®. Even after using high masses of sample, nearly 258 mg, the adsorption properties of the mask were quite poor, and showed a surface area of just 0.25 $m^2 g^{-1}$. Thus, we infer from these results that the chiffon fabric, being a woven material with even larger mesh openings, would have not presented a much higher surface area, although it was more flexible than the commercial Whatman filter. Thus, we further substantiate that an inserted electrospun Nylon material into existing commercial face masks, such as the one tested from Kimberly-Clark®, could potentially help increase the effectivity of exhaled particle retention, while still remaining flexible in use. This method could make it possible to introduce fabricate nonelectronic, wearable diagnostic masks in the future.

Nongrafted Electrospun Membranes Outperform the Commercial Controls

From Figure 3(B), we see that the pure electrospun Nylons: 10CM SM, and 10CM NSM had the least salt aerosol losses to the waste conductivity container. Overall, the conductivity changes observed when using the electrospun membranes were up to five times less than those observed from using the commercial Whatman filter papers. This suggests that the most aerosol could be captured here using these membranes, and correlates to the 95% capture efficiency shown in Figure 4 derived from eqs. (1) through (3). As shown in Table II, their high surface areas were contributing factors to these results. At best, after being thoroughly dried post production, the areas ranged from 44 to 58 $m^2 g^{-1}$. These values are in accordance with the surface areas expected from permeable nanofiber media with fiber diameters between 100 and 150 nm.[30–32]

As these two electrospun Nylon types had no visible mechanical failures during the 45-min salt aerosol capture trials, we determined them to be the most mechanically stable, and optimally performing, under wet conditions. While the 12.5CM membrane did not show any evidence of large damage after the aerosol capture trials, it captured nearly 10% less salt content with a slightly higher error than that of the other two nongrafted membranes. Overall, these differences in the capture efficiency, compared to the commercial controls, were mainly due to the high distributions of nanosized interfiber mesh-hole openings, nanofiber diameters, and the tensile strengths, found for each membrane produced.

Capture Efficiencies are Enhanced by the Properties in Nongrafted Electrospun Media. The three 15 cm × 93 cm membranes were produced using the same polymer concentrations, but under different processing conditions (Table I). As there is no relevant literature, to our knowledge, discussing the differences between the fiber morphology and tensile strength of large scale Nylon membranes arising from changes in electrospinning parameters, we attempted to produce the best membrane for exhaled saline aerosol capture while systematically studying the produced membrane properties. The production of large scale nanofiber media was desired to eliminate variability arising from multiple, smaller membranes produced, as the electrospinning process is known to be affected by shifts in ambient temperature and humidity.

Morphologically, all membranes contained evenly distributed smooth, cylindrical fibers without broken filaments or beads. The black line graph in Figure 6 shows that fibers spun from the shortest needle to collector distance, without a sliding mechanism (10CM NSM), were the largest. Adding the sliding mechanism decreased the diameter by about 20 nm (10CM SM), and finally, increasing the needle to collector distance to 12.5 cm 12.5CM SM) further decreased the diameter by another 20 nm. Ultimately, these differences arose from the placement

ID: kannanb Time: 13:28 I Path: //chenas03/Cenpro/ApplicationFiles/Journals/Wiley/APP#/Vol00000/161191/Comp/APPFile/JW-APP#161191

J_ID: z8e Customer A_ID: APP44759 Cadmus Art: APP44759 Ed. Ref. No.: APP-2016-10-1584.R1 Date: 31-December-16 Stage: Page: 10

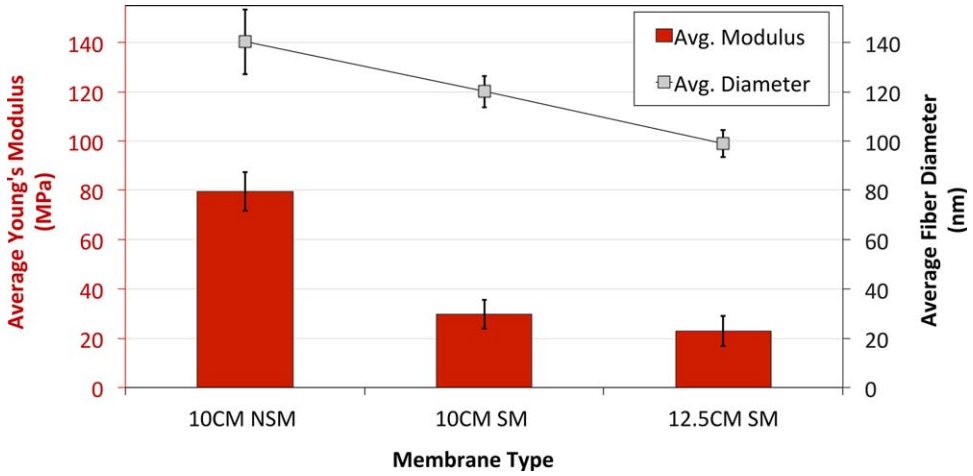

Figure 6. The average Young's Modulus (left *y*-axis, red bar graph), and the average fiber diameter (right *y*-axis, black line graph) of all three electrospun Nylon membrane types (10CM NSM, 10CM SM, and 12.5CM SM), with respective 95% confidence interval error bars, are shown in the same plot. [Color figure can be viewed at wileyonlinelibrary.com]

of the needles (varying the needle-tip-to-collector distances from 10 cm to 12 cm), and the use of the axial slide below the collector (varying the distribution of the nonwoven fibers collected).

From SEM analysis, we also saw that samples from membrane 10CM NSM had a significant quantity of thicker filaments (ranging from 300 nm to 700 nm) dispersed throughout. We hypothesize this may have contributed to increasing the Young's Modulus determined from the Instron elongation tests. Figures S.2 and S.3(A–C) in the Supporting Information show the relevant stress–strain curve data, and SEM images, respectively. Furthermore, the presence of these filaments suggested that without a sliding mechanism added to the drum, the fibers created were not as uniform in size, although macroscopically, 10CM NSM had a uniform distribution of fiber content overall. The axial slide enabled a far better distribution of fiber coverage on the aluminum collector, as well as the expected thinner fibers with an increased needle-tip-to-collector distance.[52] With thinner fibers produced, decreased average Young's modulus was also observed (Figure 6, bar graph). Macroscopically, the membrane containing the smallest fiber diameters, 12.5CM SM, also was thinner and appeared nearly translucent compared to the two 10CM samples (Figure 7). Therefore, in addition to thinner fibers collected, less fiber concentration per area may have also played a role in decreasing the modulus. F7

While we expected some significant membrane degradation to have occurred for the 10CM SM samples during aerosol capture, given that its modulus was lower than 10CM NSM, it seems like it performed similarly. Two reasons for this may be that the flexibility that all the electrospun Nylon membranes inherently had, along with the particular 120 nm average diameter fibers from the SM sample, were enough to make the SM sample stable enough for aerosol capture without extra thicker filaments necessary. For the 12.5CM SM membrane, this was not the case, however, as too thin fibers could not contribute to maintaining the membrane's resiliency during aerosol capture.

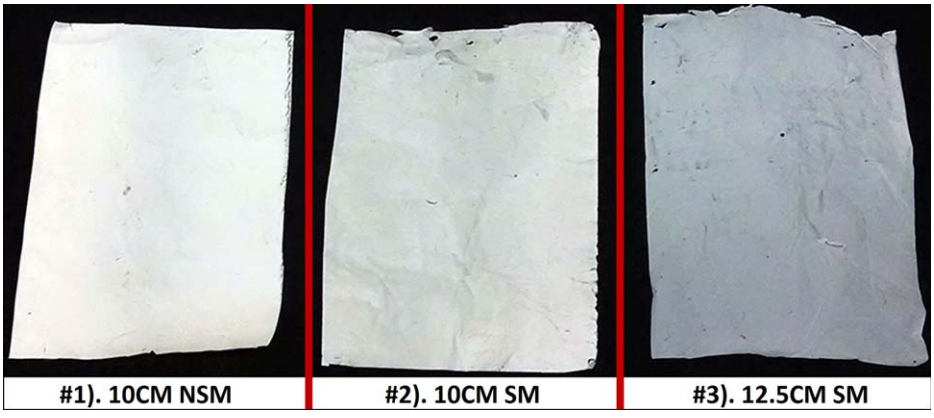

Figure 7. The macroscopic differences between samples of the three electrospun large scale membranes laid over a black background. Membrane 12.5CM SM shows highest transparency and is physically the thinnest. All samples shown here are 2 cm × 4 cm cut rectangles. [Color figure can be viewed at wileyonlinelibrary.com]

ID: kannanb Time: 13:28 I Path: //chenas03/Cenpro/ApplicationFiles/Journals/Wiley/APP#/Vol00000/161191/Comp/APPFile/JW-APP#161191

J_ID: z8e Customer A_ID: APP44759 Cadmus Art: APP44759 Ed. Ref. No.: APP-2016-10-1584.R1 Date: 31-December-16 Stage: Page: 11

The Sizes of Electrospun Membrane Mesh-Holes are Confirmed via Two Methods. Finally, the mesh-hole openings between fibers in the electrospun membranes were important factors leading to high aerosol retention. The mesh-holes of the electrospun and grafted materials were observed using two methods: capillary flow porometry, and SEM image analysis via estimative ImageJ binary pixel exclusion. Both methods have been used throughout the membrane science and biology fields, interchangeably, for estimating inter-fiber mesh-hole sizes in three-dimensional filamentous materials, and several reviews regarding their validity have been documented.[53–55]

Although the process of Image J mesh-hole size analysis by thresholding SEM fiber images into binary masks is subject to error depending on how the binary mask is discriminated, and the quality of images used, the relative agreement in the mesh-hole sizes we determined here, to those experimentally found via porometry, is quite decent when used primarily as an estimative approach. We caution, however, that that the Image J technique should never replace empirical measurements used for gathering mesh opening information from membranes physically, unless the samples are too sensitive to be tested through experimental means. For testing other levels of hierarchical intraporosity in materials, additional methods in mass transport and adsorption through the pores should be employed.

However, for our study of micro-particle aerosol breath capture by fibrous membranes, the analysis of the mesh-hole openings present throughout will suffice. Here, we use the Image J technique only as a first approximation of the openings visible by SEM in the grafted sample. Our experimental tests of these mesh-hole distributions using the capillary flow porometry technique were performed separately. The plots in Figure 8(A–D) show the percentage of mesh-holes found per membrane for various area diameters measured using Image J analysis for just the electrospun materials, and porometry for both the electrospun materials, and controls. F8

The grafted membrane was not able to be tested using porometry due to its brittle nature. Likewise, the nonwoven Whatman filter paper was not analyzed through the Image J process due to the larger variability, and overlapping nature of the meshes present in this membrane. Hotaling *et al.* have suggested several guidelines for choosing the most appropriate SEM images that can be used for binary, and mesh-hole size segmentation.[55]

The controls in Figure 8(B,C) show a much higher distribution of mesh-holes normally distributed nearer to 110 μm for the woven, and 6 μm for the nonwoven textiles, respectively. Although, from Figure 5, the nonwoven Whatman was able to capture nearly 70% of the salt sized at 1.55 μm, we suspect that this may have already been due to particle and wet droplet accumulation during the aerosol capture process. The immediate decrease in percentage seen afterwards, in addition to the results from Figure 3(A), indicated rupture in the Whatman filter paper. Also, from the surface area analysis, nitrogen adsorption was far lower for the controls than for the electrospun materials.

Using the same porometry testing method as for the controls above, the nongrafted electrospun materials, shown in Figure 8(A), were found to have a more skewed distribution of mesh-holes sized towards 114 nm to 119 nm. According to Li *et al.* even a small increase in nanofiber membrane thickness and mass can contribute to an increased percentage of smaller sized interfiber mesh openings. Membrane 10CM NSM, as seen from the tensile and SEM data presented above, had much higher strength and a slightly higher portion of thicker filaments, thus, it makes sense that it should have a higher distribution of slightly smaller individual mesh-holes. This provides further justification for how these membranes were able to perform better than the controls during the aerosol capture studies discussed in the Results section.

A quick comparison between these mesh-hole sizes, and those in the grafted samples, determined using the Image J estimation method show that the grafted membranes may have had more mesh-holes nearer to 50 nm in size, rather than a larger distribution skewed toward the hundred nanometer range. While it could provide reasoning as to why this membrane was able to capture the aerosol content sized at 1.55 μm, and at 0.52 μm, Figure 8(D) still shows there is quite some variability in the mesh-hole sizes detected using this technique. For example, the percentage of mesh-hole openings detected here for the nongrafted membranes is still quite low when compared to those observed experimentally.

At best, we can only approximate, based on the reduced surface area observed for the grafted membranes, and the SEM images presented in Figure 9(A,D), that reduced interfiber mesh-holes may have contributed to the better capture of the micron and submicron salt aggregates from the exhaled aerosol. Aside from these two aspects, the grafted membrane had the lowest overall capture efficiency of the electrospun membranes. The following section further discusses why the grafting process may have failed, and why the lower aerosol capture was observed. F9

Grafted Membrane Properties Reduce Sustained Aerosol Capture

Although the gamma irradiation induced acrylic acid grafting process was successful, as seen from the SEM images shown in Figure 9(A,D) [in comparison with their original appearance in Figure 9(B)], and from the FTIR analysis obtained [shown in the Supporting Information, Figure S.6(A,B)], the total aerosol captured on the grafted membranes was quite low. Moreover, the membranes became very brittle, and could not retain aerosol content consistently, as the conductivity results in Figure 3(B) show. Membrane shrinkage was also observed [Figure S.1(C), of the Supporting Information]. This was not expected as a previous study has shown that nanofibers could be exposed to twice the amount of gamma radiation intensity used here, without experiencing changes in either fiber diameter or fiber mesh-hole sizes.[56]

However, here it is clear that the combined mutual exposure to both elements—irradiation and acrylic acid monomer, contributed to the poor aerosol capture seen. Specifically, the development of polymerized films and beads of acrylic acid, as well as

ID: kannanb Time: 13:28 I Path: //chenas03/Cenpro/ApplicationFiles/Journals/Wiley/APP#/Vol00000/161191/Comp/APPFile/JW-APP#161191

J_ID: z8e Customer A_ID: APP44759 Cadmus Art: APP44759 Ed. Ref. No.: APP-2016-10-1584.R1 Date: 31-December-16 Stage: Page: 12

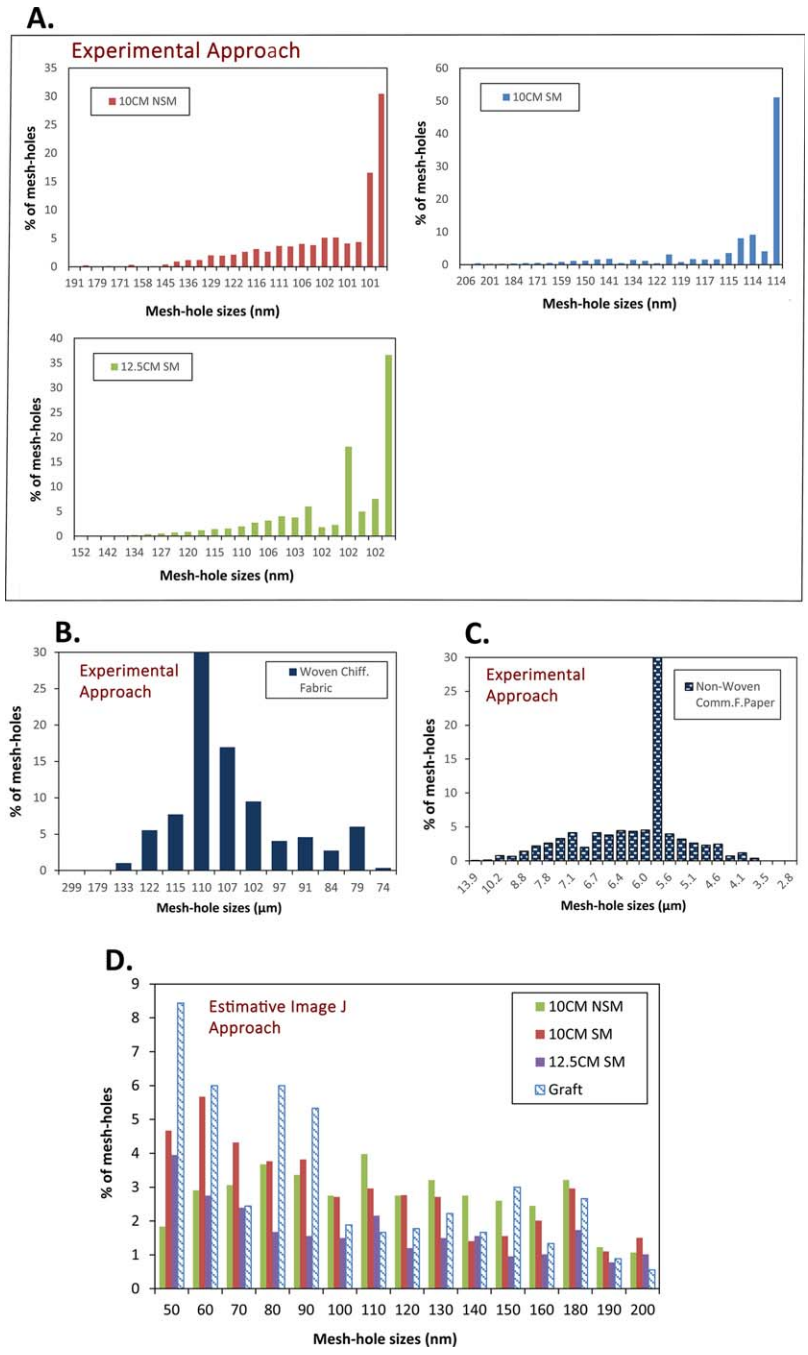

Figure 8. The percentage of mesh-holes in the membranes were observed using two different methods: capillary flow porometery ("experimental approach"), and Image J binary SEM image analysis ("estimative Image J approach"). The electrospun membranes were analyzed using both methods, shown in plots (A) and (D). The control membranes (woven chiffon fabric, and nonwoven Whatman paper) were analyzed through only the experimental technique, shown in plots (B), and (C), respectively. More information regarding these techniques and a basic numerical mean mesh-hole size calculation comparison can be found in the Supporting Information, p 6–7. [Color figure can be viewed at wileyonlinelibrary.com]

fiber coagulation from degradation [Figure 9(D)], lowered the surface area of the membrane. The SEM image of the membrane shown in Figure 9(C), exposed to 20 min of irradiation, drastically displays the effects of deeper acrylic acid integration within the membrane if it is polymerized for an extended period of time. Rougher and thicker surface textures form throughout each filament.

Ultimately, while the grafted membranes would not be practically useful for integration as diagnostic substrates within commercial face masks, as they have low durability and surface area, it was interesting to find that in comparison to the commercial Whatman filter paper performance, higher percentages of aerosol content sized at 1.55 µm, and at 6.0 µm were capturable (Figure 5). Again, we can only estimate that this could have been due to a

ID: kannanb Time: 13:28 I Path: //chenas03/Cenpro/ApplicationFiles/Journals/Wiley/APP#/Vol00000/161191/Comp/APPFile/JW-APP#161191

J_ID: z8e Customer A_ID: APP44759 Cadmus Art: APP44759 Ed. Ref. No.: APP-2016-10-1584.R1 Date: 31-December-16 Stage: Page: 13

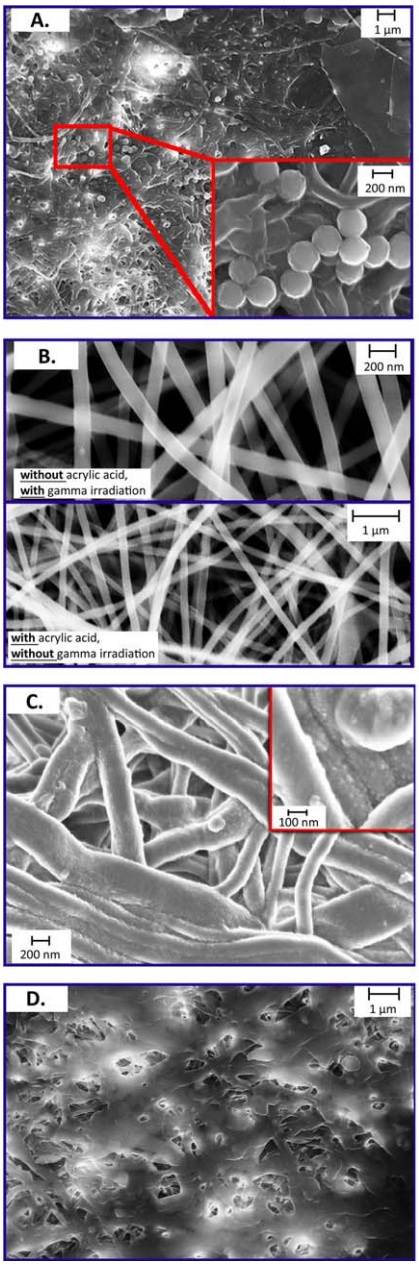

Figure 9. Representative SEM images of electrospun Nylon membranes (10CM NSM and 10CM SM) after being grafted with acrylic acid via gamma irradiation are shown. The reduction of open mesh area by the formation of polymerized spheres over the membrane surfaces is shown in (A) and (D), after irradiation and acrylic acid exposure for 1 min. The membranes without acrylic acid exposure, with irradiation for 1 min, and with acrylic acid exposure for 1 min, without irradiation, are shown in (B) as the controls. The severity of effects from exposing both gamma irradiation and acrylic acid on one membrane for 20 min is shown in (C). The irradiation dosage for all the membranes was 523 rad min^{-1}. [Color figure can be viewed at wileyonlinelibrary.com]

reduction in the mesh-hole sizes observed from the data in Figure 9(D). However, further experimentally based analyses of the level of mesh degradation in these types of membranes would have to be performed for confirmation.

The grafting data, and consequent results in exhaled aerosol capture efficiency for the grafted sample, are significant in that we can now confirm the morphological traits of these electrospun membranes are not as amenable to high level post-treatments as once believed. While the nontreated electrospun materials can function better than commercial paper-like textiles, if further alterations to the chemical structure postfabrication are performed, such as gamma irradiation initiated grafting, the robustness they once had may be compromised. Although it is highly unlikely that electrospun membranes could encounter such harsh environments if ever integrated into face mask textiles, it would be interesting if future studies can show how consistent their capture efficiencies can remain, when combined with lateral flow, or colorimetric assay type functions, for use in real-time breath diagnosis.

Finally, grafting Nylon nanofiber media using other methods such as plasma treatments, or by chemical cross-linkers, may provide the ability to fine-tune mesh and fiber diameter sizes postelectrospinning without causing the losses in membrane stability observed here. The variation of the electrolytic properties of spun nanofiber membranes for antibody functionalization has already proved successful.[57] Furthermore, a series of stacked membranes with tailored morphologies, perhaps even assembled using other design processing techniques such as ultra-sonic bonding, may provide initial solutions for the first prototypes in light weight, highly flexible, and sensor driven face-mask design.[44]

CONCLUSIONS

Our study has shown that the morphological characteristics of large-scale (15 cm × 93 cm), and uniformly thick, electrospun Nylon-6 fiber membranes may be suitable for implementation as light weight diagnostic devices for capturing exhaled breath aerosols. The electrospun membranes here captured 39% to 50% more simulated exhaled breath, and 60% to 95% of aerosol droplets in the inhalable 0.2 μm to 6 μm size range, when compared to other commercial woven and nonwoven controls used. The crucial morphological traits in the electrospun membranes which greatly influenced their better performance were: surface area, interfiber mesh-hole size, and fiber diameter size. Likewise, these attributes were all found to be tunable from the specific parameters chosen for fabricating the membranes tested for aerosol capture. Unlike the controls, the nongrafted electrospun membranes did not rupture during aerosol capture, nor did they display signs of degradation, despite weighing 20 times less. Furthermore, our study has also shown that the large electrospun sheets can be produced within 2 to 4 h, and with minimal consumption of polymer solution (up to 10 mL of 20 wt % Nylon in solvent, per large sheet).

Alternatively, though the grafting of acrylic acid onto the selected electrospun membranes using gamma irradiation was successful. This led to decreased mesh openings, surface area, and strength in the membranes. While we suspect that the decrease in mesh-holes may have led to a better capture of 1.55 μm sized aerosol salt particles, the inability of the membranes to endure the full duration of the aerosol dispersal trials without breaking show

ID: kannanb Time: 13:28 I Path: //chenas03/Cenpro/ApplicationFiles/Journals/Wiley/APP#/Vol00000/161191/Comp/APPFile/JW-APP#161191

J_ID: z8e Customer A_ID: APP44759 Cadmus Art: APP44759 Ed. Ref. No.: APP-2016-10-1584.R1 Date: 31-December-16 Stage: Page: 14

that these grafted membranes are not currently suitable for face mask integration. Instead, for this application, the aforementioned nongrafted electrospun Nylon membranes are recommended as they were easily electrospinnable in bulk, and displayed consistent aerosol capture efficiency and resiliency. Furthermore, they show potential for acting as carrier substrates for future diagnostic functions in face masks without the risks for compromising breath capture overall.

ACKNOWLEDGMENTS

This work made use of the Cornell Center for Materials Research (CCMR) supported through the NSF MRSEC program (DMR-1120296). Thanks are extended to Sam Zeng, Mick Thomas, Brian Williams, and Joe Carlin for the valuable instrumentation assistance and training. Thanks are also extended to Nidia Trejo, and Stéphane Corgié, for the valuable advice and discussions. Finally, the authors also thank Ken Kemphues for allowing our access to the gamma irradiation facility located in the Department of Molecular Biology and Genetics at Cornell University.

REFERENCES

1. Lindsley, W. G.; Blachere, F. M.; Thewlis, R. E.; Vishnu, A.; Davis, K. A.; Cao, G.; Palmer, J. E.; Clark, K. E.; Fisher, M. A.; Khakoo, R.; Beezhold, D. H. *PLoS One* **2010**, *5*, e15100.
2. Weber, T. P.; Stilianakis, N. I. *J. Infect.* **2008**, *57*, 361.
3. Milton, D. K.; Fabian, M. P.; Cowling, B. J.; Grantham, M. L.; McDevitt, J. *J. PLoS Pathog.* **2013**, *9*, e1003205.
4. Li, K. S.; Guan, Y.; Wang, J.; Smith, G. J. D.; Xu, K. M.; Duan, L.; Rahardjo, a. P.; Puthavathana, P.; Buranathai, C.; Nguyen, T. D.; Estoepangestie, a. T S.; Chaisingh, A.; Auewarakul, P.; Long, H. T.; Hanh, N. T. H.; Webby, R. J.; Poon, L. L. M.; Chen, H.; Shortridge, K. F.; Yuen, K. Y.; Webster, R. G.; Peiris, J. S. M. *Nature* **2004**, *430*, 209.
5. Thompson, K. A.; Pappachan, J. V.; Bennett, A. M.; Mittal, H.; Macken, S.; Dove, B. K.; Nguyen-Van-Tam, J. S.; Copley, V. R.; O'Brien, S.; Hoffman, P.; Parks, S.; Bentley, A.; Isalska, B.; Thomson, G. EASE Study Consortium. *PLoS One* **2013**, *8*, e56278.
6. Lindsley, W. G.; Blachere, F. M.; Beezhold, D. H.; Thewlis, R. E.; Noorbakhsh, B.; Othumpangat, S.; Goldsmith, W. T.; McMillen, C. M.; Andrew, M. E.; Burrell, C. N.; Noti, J. D. *Influenza Respir. Viruses* **2016**, *10*, 404.
7. Cowling, B. J.; Ip, D. K. M.; Fang, V. J.; Suntarattiwong, P.; Olsen, S. J.; Levy, J.; Uyeki, T. M.; Leung, G. M.; Malik Peiris, J. S.; Chotpitayasunondh, T.; Nishiura, H.; Mark Simmerman, J. *Nat. Commun.* **2013**, *4*, 1935.
8. Lindsley, W. G.; Pearce, T. A.; Hudnall, J. B.; Davis, K. A.; Davis, S. M.; Fisher, M. A.; Khakoo, R.; Palmer, J. E.; Clark, K. E.; Celik, I.; Coffey, C. C.; Blachere, F. M.; Beezhold, D. H. *J. Occup. Environ. Hyg.* **2012**, *9*, 443.
9. Tellier, R. J. R. *Soc. Interface* **2009**, *6*, S783.
10. Yang, W.; Marr, L. C. *PLoS One* **2011**, *6*, e21481.
11. Yang, S.; Lee, G. W. M.; Chen, C. M.; Wu, C. C.; Yu, K. P. *J. Aerosol Med.* **2007**, *20*, 484.
12. Yang, W.; Elankumaran, S.; Marr, L. C. *J. R. Soc. Interface* **2011**, *8*, 1176.
13. Hall, C. B. *J. Infect. Dis.* **2013**, *207*, 1027.
14. Centers for Disease Control. Measles, Signs and Symptoms; CDC. Available at: http://www.cdc.gov/measles/about/signs-symptoms.html. Last accessed September 4, **2016**.
15. Centers for Disease Control. Pertussis, Whooping Cough, Signs and Symptoms; CDC. Available at: http://www.cdc.gov/pertussis/about/signs-symptoms.html. Last accessed September 4, **2016**.
16. McCracken, G. H. *Pediatr. Infect. Dis. J.* **2000**, *19*, 924.
17. Ortega-Sanchez, I. R.; Molinari, N. A. M.; Fairbrother, G.; Szilagyi, P. G.; Edwards, K. M.; Griffin, M. R.; Cassedy, A.; Poehling, K. A.; Bridges, C.; Staat, M. A. *Vaccine* **2012**, *30*, 4175.
18. Thursky, K.; Cordova, S. P.; Smith, D.; Kelly, H. *J. Clin. Virol.* **2003**, *27*, 170.
19. Romeo, A.; Leung, T. S.; Sánchez, S. *Lab Chip* **2016**, *16*, 1957.
20. Fabian, P.; McDevitt, J. J.; Houseman, E. A.; Milton, D. K. *Indoor Air* **2009**, *19*, 433.
21. Diaz, K. T.; Smaldone, G. C. *Am. J. Infect. Control* **2010**, *38*, 501.
22. Jefferson, T.; del Mar, C.; Dooley, L.; Ferroni, E.; Al-Ansary, L. A.; Bawazeer, G. A.; van Driel, M. L.; Nair, S.; Foxlee, R.; Rivetti, A. *Health Technol. Assess. (Rockv)* **2010**, *14*, 347.
23. Burgess, A.; Horii, M. *Sociol. Health Illness* **2012**, *34*, 1184.
24. Oberg, T.; Brosseau, L. M. *Am. J. Infect. Control* **2008**, *36*, 276.
25. MacIntyre, C. R.; Cauchemez, S.; Dwyer, D. E.; Seale, H.; Cheung, P.; Browne, G.; Fasher, M.; Wood, J.; Gao, Z.; Booy, R.; Ferguson, N. *Emerg. Infect. Dis.* **2009**, *15*, 233.
26. Bałazy, A.; Toivola, M.; Adhikari, A.; Sivasubramani, S. K.; Reponen, T.; Grinshpun, S. A. *Am. J. Infect. Control* **2006**, *34*, 51.
27. Neilson, S. *Can. Med. Assoc. J.* **2016**, *188*, 606.
28. Brink, S. Will A Surgical Mask Keep You Safe in a Viral Outbreak? Available at: http://www.npr.org/sections/goatsandsoda/2015/06/22/416466284/will-a-surgical-mask-keep-you-safe-in-a-viral-outbreak. Last accessed August 31, **2016**.
29. Graham, J. In Flu Season, Use a Mask. But Which One? Available at: http://newoldage.blogs.nytimes.com/2013/01/16/in-flu-seasonuse-a-mask-but-which-one/?_r=0. Last accessed August 31, **2016**.
30. Ryu, Y. J.; Kim, H. Y.; Lee, K. H.; Park, H. C.; Lee, D. R. *Eur. Polym. J.* **2003**, *39*, 1883.
31. Eichhorn, S. J.; Sampson, W. W. *J. R. Soc. Interfaces* **2010**, *7*, 641.
32. Wendorff, J. H.; Agarwal, S.; Greiner, A. In Electrospinning—Materials, Processing, and Applications; Wiley-V C H Verlag Gmbh: Weinheim, Germany, **2012**; p 185.
33. Grafe, T.; Graham, K. In International Nanwovens Technical Conference; Georgia, USA, **2002**; p 24.
34. Hosseini, S. A.; Tafreshi, H. V. *Powder Technol.* **2011**, *212*, 425.

ID: kannanb Time: 13:28 I Path: //chenas03/Cenpro/ApplicationFiles/Journals/Wiley/APP#/Vol00000/161191/Comp/APPFile/JW-APP#161191

35. Wujcik, E. K.; Blasdel, N. J.; Trowbridge, D.; Monty, C. N. *IEEE Sens. J.* **2013**, *13*, 3430.
36. Blasdel, N. J.; Wujcik, E. K.; Carletta, J. E.; Lee, K. S.; Monty, C. N. *IEEE Sens. J.* **2015**, *15*, 300.
37. Guder, F.; Ainla, A.; Redston, J.; Mosadegh, B.; Glavan, A.; Martin, T. J.; Whitesides, G. M. *Angew. Chem. Int. Ed. Engl.* **2016**, *55*, 5727.
38. Li, L.; Frey, M. W.; Green, T. B. *J. Eng. Fiber. Fabr.* **2006**, *1*, 1.
39. Hossain, S. M. Z.; Luckham, R. E.; McFadden, M. J.; Brennan, J. D. *Anal. Chem.* **2009**, *81*, 9055.
40. Senthamizhan, A.; Balusamy, B.; Uyar, T. *Anal. Bioanal. Chem.* **2015**, *408*, 1285.
41. Reneker, D. H.; Yarin, A. L. *Polymer (Guildf)* **2008**, *49*, 2387.
42. Luo, C. J.; Stoyanov, S. D.; Stride, E.; Pelan, E.; Edirisinghe, M. *Chem. Soc. Rev.* **2012**, *41*, 4708.
43. Reyes, C. G.; Sharma, A.; Lagerwall, J. P. F. *Liq. Cryst.* **2016**, *43*, 1.
44. Trejo, N. K.; Reyes, C. G.; Sanchez, V.; Zhang, D.; Frey, M. W. *Int. J. Fash. Des. Technol. Educ.* **2016**, *9*, 3266.
45. Trejo, N. K.; Frey, M. *J. Appl. Polym. Sci.* **2015**, *132*, 42657.
46. Lu, P.; Xia, Y. *Langmuir* **2013**, *29*, 7070.
47. Enz, E.; Lagerwall, J. *J. Mater. Chem.* **2010**, *20*, 6866.
48. Peng, R. D. *JAMA* **2008**, *299*, 2172.
49. Salvaggio, J. E. *J. Allergy Clin. Immunol.* **1994**, *94*, 304.
50. Yin, G. B. *J. Fiber Bioeng. Informatics* **2010**, *3*, 137.
51. Minamide, L. S.; Bamburg, J. R. *Anal. Biochem.* **1990**, *190*, 66.
52. Mazoochi, T.; Hamadanian, M.; Ahmadi, M.; Jabbari, V. *Int. J. Ind. Chem.* **2012**, *3*, 2.
53. Li, D.; Frey, M. W.; Joo, Y. L. *J. Membr. Sci.* **2006**, *286*, 104.
54. Fratila-Apachitei, L. E.; Kennedy, M. D.; Linton, J. D.; Blume, I.; Schippers, J. C. *J. Membr. Sci.* **2001**, *182*, 151.
55. Hotaling, N. A.; Bharti, K.; Kriel, H.; Simon, C. G. *Biomaterials* **2015**, *61*, 327.
56. Schrote, K.; Frey, M. W. *Polymer (Guildf)* **2013**, *54*, 737.
57. Matlock-Colangelo, L.; Coon, B.; Pitner, C. L.; Frey, M. W.; Baeumner, A. *J. Anal. Bioanal. Chem.* **2016**, *408*, 1327.

SGML and CITI Use Only
DO NOT PRINT